# Cell Death & Disease

## Article in Press

# Unveiling ZNF124 as a novel determinant in neurodegeneration: orchestration of photoreceptor homeostasis through MSX2 transcriptional regulation

Yeming Yang, Xiaoyan Jiang, Shujin Li, Kuanxiang Sun, Rong Zou, Can Chen, Yi Shi, Wenjing Liu, Periasamy Sundaresan, Lulin Huang, Lin Zhang, Zhenglin Yang & Xianjun Zhu

We are providing an unedited version of this manuscript to give early access to its findings. Before final publication, the manuscript will undergo further editing. Please note there may be errors present which affect the content, and all legal disclaimers apply.

If this paper is publishing under a Transparent Peer Review model then Peer Review reports will publish with the final article.

# Unveiling ZNF124 as a Novel Determinant in neurodegeneration: Orchestration of Photoreceptor Homeostasis through MSX2 Transcriptional Regulation

Yeming Yang[1,2#], Xiaoyan Jiang[1#], Shujin Li[1-3#], Kuanxiang Sun[1#], Rong Zou[1#], Can Chen[1], Yi Shi[1], Wenjing Liu[1], Periasamy Sundaresan[4*], Lulin Huang[1,2*], Lin Zhang[1-3*], Zhenglin Yang[1-3*], Xianjun Zhu[1-3,5*]

[1]Genetic Diseases Key Laboratory of Sichuan Province, Center for Medical Genetics, Sichuan Provincial People's Hospital, School of Medicine, University of Electronic Science and Technology of China, Chengdu, Sichuan, 610072, China;

[2]Research Unit for Blindness Prevention of Chinese Academy of Medical Sciences (2019RU026), Sichuan Academy of Medical Sciences and Sichuan Provincial People's Hospital, Chengdu, Sichuan, 610072 China;

[3]Sichuan-Chongqing Joint Key Laboratory for Pathology and Laboratory Medicine, Jinfeng Laboratory, Chongqing, 401329, China;

[4]Department of Genetics, Aravind Medical Research Foundation, Aravind Eye Hospital, Madurai, Tamil Nadu, India;

[5]Henan Eye Hospital, People's Hospital of Zhengzhou University, Henan Provincial People's Hospital, Zhengzhou, 450003, China.


#These authors contributed equally to this work: Yeming Yang, Xiaoyan Jiang, Shujin Li, Kuanxiang Sun, Rong Zou.

**To whom correspondence should be address:** to Dr. Xianjun Zhu, e-mail: xjzhu@uestc.edu.cn; Dr. Zhenglin Yang, yangzhenglin@cashq.ac.cn; Dr Lin Zhang, zhanglin202@uestc.edu.cn, Dr. Lulin Huang, huangluling@yeah.net, Genetic Diseases Key Laboratory of Sichuan Province, Sichuan Provincial People's Hospital, University of Electronic Science and Technology of China, Chengdu, Sichuan, 610072, China; or sundar@aravind.org, Department of Genetics, Aravind Medical Research Foundation, Aravind Eye Hospital, Madurai, Tamil Nadu, India.

# Abstract

Retinitis pigmentosa (RP), affecting more than 20 million people worldwide, refers to a group of inherited retinal dystrophies characterized by progressive photoreceptor degeneration and vision loss. However, the underlying genetic causes of substantial RP cases remain unidentified. In this report, we identified a novel homozygous splicing variant, c.219-1delG, which introduced skipping of exon 4 of the *ZNF124* gene in a large RP pedigree by whole exome sequencing analysis. To elucidate the pathogenesis of the mutation, we generated a retina-specific knockout mouse model of ZNF124 murine homologous gene *Gm20541*, which manifested RP-like phenotypes characterized by reduced electroretinogram response and progressive retinal degeneration. Integrated analysis using CUT&Tag, ChIP-exo, and RNA-seq data further revealed that ZNF124 regulated MSX2 expression through binding its promoter region. Moreover, deletion of *Msx2* in the retina led to thinning of retina owing to progressive degeneration of rod cells. Integrated analysis of RNA-seq data from both *Gm20541* and *Msx2* mutant retinas indicated that ZNF124 is essential for maintaining normal retinal function by regulating *Msx2* transcription, which in turn controls the expression of murine homologues of retinal dystrophy genes *Rs1*, *Pde6g*, and *Pdc*. Taken together, our study identified a novel mechanism of transcriptional regulation for retinal homeostasis via ZNF124-MSX2 axis and ZNF124 as a novel candidate gene for RP.

# Introduction

Retinitis pigmentosa (RP；OMIM:26800) refers to a group of hereditary degenerative diseases of the retina characterized by night blindness, a gradual constriction of peripheral visual field initially, followed by impairment of central vision and ultimately legal blindness[1]. Progressive loss of photoreceptors (including both rods and cones) is the primary underlying cause for the progressive vision loss in RP

pathologies[2,3]. As a genetically heterogeneous disease, RP is linked to various genes and can be inherited in different ways, such as autosomal-dominant (adRP, 30-40%), autosomal-recessive (arRP, 50-60%) or X-linked (5-15%) manners[4]. Moreover, non-Mendelian inheritance patterns, including digenic and maternal inheritances, have also been reported to account for very few cases[5,6]. Until present, according to the RetNet database (https://sph.uth.edu/retnet/), over 80 genes have been implicated in non-syndromic forms of RP, most of which are preferentially expressed in retinal photoreceptors and encode various proteins involved in the phototransduction cascade, the metabolic pathway, the photoreceptor structure, or transcription regulation. However, these identified genes can only account for approximately 50-60% of existing RP patients, and the genetic causes for nearly 40% of RP cases remain undetermined. To this end, more unknown RP associated pathogenic genes and underlying mechanisms are expected to be uncovered.

Zinc-finger (ZNF) proteins containing the Krüppel-associated box (KRAB-containing proteins) are the largest single family of transcription factors (TFs) in mammals, which play an essential role in cell differentiation, cell proliferation, apoptosis, and neoplastic transformation[7,8]. Here we identified a novel candidate gene associated with autosomal recessive RP, ZNF124, encoding a KRAB-related zinc finger protein of 351 amino acids that is predicted to harbor seven C2H2-type finger binding domains thought to be implicated in DNA binding[9]. ZNF124 gene consisted of 4 exons and 3 introns, which mapped to chromosome 1q44, and alternative splicing results in multiple transcript variants encoding distinct proteins. Research on the function of ZNF124 remains limited at present. A previous study cloned *ZNF124* and identified it as a transcription factor, which was involved in the inhibitory effect of VEGF on apoptotic cell death in human hematopoietic cells[10]. In terms of pathogenesis, ZNF124 has been associated with the progression of head and neck squamous cell carcinoma (HNSCC)[11] as well as highly aggressive

medulloblastomas[12]. In the nervous system, ZNF124 was reported as a candidate gene for the Dandy-Walker complex (DWC) in human[13]. Regrettably, its exact functions have not been elucidated in vivo yet.

Muscle segment homeobox 2 (MSX2), a homeobox-containing transcription factor, which dysregulation has been implicated in developmental anomalies of several types of tissues, including craniofacial tissues, hair follicles, teeth, heart, and brain[14-16]. Intriguingly, MSX2 appears to have dual functions in regulating apoptosis and retinal fate determination. For example, overexpression of *Msx2* in mice has been shown to induce microphthalmia and optic nerve aplasia by suppressing *Bmp4* expression in the optic vesicle before lens induction. Increased retinal apoptosis combined with reduced proliferation finally leads to retinal thinning and microphthalmia[17]. Conversely, disruption of *Msx2* during early neurulation also results in hypoplasia of the maxillary, mandibular, and frontonasal prominences, as well as abnormalities in the somite, neural tube, and eye. Eye defects are characterized by enlarged optic vesicles, which may ultimately contribute to microphthalmia. This conflict suggested that the normal activity of MSX2 may establish a balance between survival and apoptosis of neural crest-derived cells required for proper craniofacial morphogenesis[18]. Additionally, *Msx2* overexpression reduces the expression of retinal ganglion cell (RGC)-specific differentiation markers *Math5* and *Brn3b*, indicating that Msx2 influences RGC fate commitment and differentiation by delaying the timing of cell cycle exit of retinal progenitors[19]. Previous findings also indicated that *Msx2* gene is critically involved in anterior segment development and lens formation during early eye development, which finally contributes to the failure of retina folding and microphthalmia.[20,21]. These evidences highlighted that the key regulating effect of MSX2 in the developmental process of the vertebrate eye. However, whether MSX2 plays a role in neuroretina at adult stage is still unclear.

In the current study, we report a novel homozygous splicing mutation (c.219-1delG) of *ZNF124* in a family suffering from RP. Detailed cDNA analysis demonstrated a 9 bp skipping across exon 3 and 4 in the patient's *ZNF124* transcript. To investigate the in vivo roles of *ZNF124* in retina, we first confirmed *Gm20541* as the homologous gene of *ZNF124* in mice, and subsequent knockout study of this murine homologous gene manifested an RP-like phenotypes characterized by reduced electroretinogram response and retinal degeneration in mice. By using CUT&Tag, ChIP-exo, and RNA-seq studies, we further revealed that ZNF124 regulated MSX2 expression through a direct binding of its promoter region. Moreover, rod-specific knockout of *Msx2* also led to apparently thinning of retinal outer nuclear layer (ONL) owing to comprehensive degeneration of rod cells. Integrated analysis of bulk RNA-seq data from both *Gm20541* and *Msx2* mutant retinas reveals that ZNF124 is essential for maintaining normal retinal function by regulating *Msx2* transcription, which in turn controls the expression of retinal disease homologous genes *Rs1*, *Pde6g*, and *Pdc*. Collectively, our findings identify *ZNF124* as a novel candidate gene associated with retinitis pigmentosa (RP) and provide molecular insights into its underlying mechanisms, highlighting its functional significance in the retina.

## Results

### Identification of a novel pathogenic splicing variant in *ZNF124* in a large arRP consanguineous family

In the present study, two probands affected with RP from one consanguineous family were recruited (Fig. 1A). Both RP probands exhibited typical RP clinical features, including early-onset night blindness, gradually decreased vision acuity, and loss of peripheral visual field. No abnormalities were observed in other organs or systems, and the overall physical development of the probands was normal. The clinical examinations of patients IV:4 (12 years old) and IV:5 (14 years old) as well as their parents III:3 and III:4 were shown in Fig. 1B. Fundus examination showed the loss of

pigment epithelial with narrowed arterioles, pale optic disk and irregular pigment clumps with both peripheral retina and macula involved in both eyes, while their parents exhibited normal structure of fundus (Fig. 1B). Optical coherence tomography (OCT) examination, which provides an indirect measure of axonal and neuronal injury in the anterior visual pathways, revealed disorganized photoreceptor layers and severely thinner retina compared to their unaffected parents (Fig. 1B). Visual field test on patient IV:4 further revealed loss of peripheral vision in both eyes (Fig. 1C), and weak response to light stimulus in both eyes was presented upon electroretinogram examination (Fig. 1D), indicating significant impairment of visual function.

To determine the causative mutations in this RP family, we conducted whole exome sequencing (WES) on genomic DNA from the proband patients IV:4 and IV:5, along with their unaffected father III:3. In total, we identified 9,366 and 9,535 nonsynonymous SNPs, as well as 452 and 449 coding indels in subject IV:4 and IV:5, respectively, which may affect amino acid sequences (Additional file 1). Among these, four homozygous regions shared by two patients (IV:4 and IV:5) were identified (Fig. S1A). We then compared the variants in these homozygous regions with well-known RP-causing genes (https://sph.uth.edu/Retnet/), and no variants of these RP genes were found in these patients. By filtering these variants against the SNP database dbSNP137, and 1000 Genome Project as well as our in-house WES control database[22,23], we exclude the variants with high frequency ($>$1%). After excluding heterozygous variants and synonymous variants, and considering the pathogenicity of variant and their retinal expression profile, a homozygous variant, c.219-1delG, in *ZNF124* gene was identified as the most likely candidate for the cause of RP disease in this family (Additional file 2). Subsequent Sanger sequencing analysis confirmed complete co-segregation of the mutations with the disease phenotype in the consanguineous family: the homozygous splicing mutation c.219-1delG in the two affected patients (IV:4 and IV:5) was verified (Fig. 1E). The parents

(III:3 and III:4) were unaffected carriers, each harboring a heterozygous variant (Fig. 1E). In contrast, the unaffected sister of the two probands did not carry this mutation (Fig. S1B). Importantly, this splicing variant was not found in the Genome Aggregation Database (https://gnomad.broadinstitute.org/) as well as the human gene mutation database (http://www.hgmd.org/), indicating that this variant was novel. Moreover, the c.219-1delG variant located at the 3' border before Exon 4 in *ZNF124* gene (Fig. 1F), which may disrupt the typical AG ends of eukaryotic introns recognized by the U2 spliceosome[24,25], and this site is evolutionarily highly conserved from human to zebrafish (Fig. 1G). Thus, these data revealed that a novel homozygous splicing variant c.219-1delG in *ZNF124* gene as candidate gene for this arRP family.

### *ZNF124* c.219-1delG mutant disrupted splicing and led to truncated protein

To assess the effect of the c.219-1delG mutation on splicing, we collected peripheral blood from patient IV:4 and generated cDNA by reverse transcription using extracted RNA from the leukocyte. Primers were designed for ZNF124 transcript to amplify the cDNA fragment between exon 3 and exon 4 by reverse transcription (RT)-PCR. Sanger sequencing of the PCR products from the patients and controls revealed that there was a deletion spanning exon 3 and exon 4 (10 bp) of the *ZNF124* cDNA (Fig. 1H), which demonstrated that the c.219-1delG splicing mutation in *ZNF124* gene disrupted normal splicing and led to a frameshift deletion variant of ZNF124 transcript (Fig. 1I). In contrast, the *ZNF124* cDNA sequence of their unaffected sister appeared normal (Fig. S1B). In terms of ZNF124 protein, this transcriptional deletion could result in frameshift change at the 73rd amino acid residue, Serine, and a termination codon occurred after twenty amino acid (p.S73fs20*) (Fig. 1J). The ZNF124 protein contains distinct functional domains: a KRAB-A box at its NH2 terminal and seven consecutively repeated Kruppel-type (C2H2) zinc finger motifs at carboxy terminus, which bind to DNA in a sequence-specific manner. Therefore, the

premature termination of ZNF124 protein sequence induced by the identified splicing

mutant could abolish the capacity of DNA binding (Fig. 1J), supporting that this

splicing mutation in *ZNF124* is the causative mutation for this arRP family.

**Construction of knockout mouse lines of *ZNF124* homologous gene *Gm20541***

ZNF124 has been reported as a transcriptional regulator linked to cell survival and

tumorigenesis in other cellular contexts[10,11], while its roles in the retina remain

unknown. To investigate the potential pathogenesis of these RP patients, we first

detected the retinal expression of ZNF124 by immunostaining on sections of monkey

retinas, which manifested that ZNF124 was distinctly co-localized with DAPI-labeled

nuclear in the retinal pigment epithelium (RPE), outer nuclear layer (ONL), inner

nuclear layer (INL), and ganglion cell layer (GCL) of the retina (Fig. S2A). To gain

more insight into the expression profile of ZNF124 in human retinas, we utilized

publicly available data from the Human Protein Atlas (HPA) databases

(https://www.proteinatlas.org)[26] to assess the translational expression levels of

ZNF124 in different retinal cell types. The single-cell data from HPA revealed that

ZNF124 was broadly expressed in whole retina and various retinal cell types,

especially highly enriched in rod photoreceptors (Fig. S2B, C), implying the critical

roles of ZNF124 in retinal rod cells.

In the mouse genome, there are eight homologous genes (*Loc102637111, Gm20422,*

*Gm14322, Zfp81, Zfp952, Zfp101, Gm20541, Zfp709*) aligned to the human ZNF124

gene. After alignment, *Gm20541* was considered as the closest homolog of the human

counterpart, which shared 59.43% sequence similarity and approximate molecular

size compared with ZNF124 (Fig. S3A). Hereby, we generated *Gm20541*-knockout

mice to explore the role of ZNF124 in the retina. In the constructed *Gm20541* allele,

an FRT-flanked internal ribosome entry site (IRES)-GFP reporter with an upstream

splicing acceptor and a neomycin (Neo) resistance cassette was inserted into intron 2,

and the FlAG-tagged exon 3 was flanked by two loxP sites, thus generating "knockout (KO) first" ($Gm20541^{KO\,first}$) mice (Fig. 2A). After removal of the IRES-GFP reporter and Neo cassette between FRT sites by FLP recombinase, the KO first was converted into a conditional knockout allele ($Gm20541^{flox/flox}$). Then, the $Gm20541^{flox/flox}$ mice can be crossed with a Six3-Cre driver line[27] to eliminate the exon 3 within the $Gm20541$ gene, which finally yields the retinal neural deletion mutant model ($Gm20541^{flox/flox}$, $Six3$-$cre$, hereafter named $Gm20541^{SKO}$) (Fig. 2A). Thereafter, we studied the expression pattern of $Gm20541$, which is transcriptionally expressed in mouse brain, cerebellum, liver, retina, intestine, muscle, heart, kidney and spleen (Fig. S3B, C). Western blot of tissue lysis from $Gm20541^{f/f}$ mouse using an antibody specific for the FLAG tag confirmed the robust protein expression in the heart, liver and retina (Fig. S3D, E). We, subsequently, examined the phenotypes of $Gm20541^{KO}$ $^{first}$ mice. Strikingly, while normal litter sizes and body weights (Fig. S4A) were shown, the $Gm20541^{KO\,first}$ mice displayed defects in limb development: their hindlimbs presented oligodactyly with fewer digits (Fig. S4B). In addition, $Gm20541$ pan-excision in $Gm20541^{KO\,first}$ mice also resulted in degeneration of retina layers at 8 months of age (Fig. S4C, D), highlighting its crucial roles in retina.

**Functional deficit and progressive retinal dystrophy in $Gm20541$ mutants**

To investigate the specific roles of $Gm20541$ in neuroretina, we next focus on the visual function and pathologies in conditional neural knockout $Gm20541^{SKO}$ mice. Scotopic electroretinograms (ERGs) were first performed on $Gm20541^{SKO}$ mice and controls at 12 months of age. As expected, remarkable decreases of amplitudes of both a-waves and b-waves were detected in scotopic ERG recordings in $Gm20541^{SKO}$ at each flash intensity compared with controls (Fig. 2B, E, F), reflecting compromised rod function. Likewise, the photopic a/b-wave and flicker amplitudes, which mainly reflect the circuits from cones, were also significantly reduced in $Gm20541^{SKO}$ mice (Fig. 2C, D, G), suggesting deficits in cone photoreceptors.

To determine the pathological changes underlying the impairment of visual function, histologic analysis was performed in *Gm20541$^{SKO}$* mice at different ages, and data revealed that the thickness of both the outer and inner nuclear layers were gradually decreased from 8 to 21 months of age (Fig. 3A-F), accompanied by a shortened outer segment (OS). By 21-month-old, a nearly 57.34% decrease in ONL thinness was detected compared to that in control retinas (Fig. 3C, F), indicating massive loss of photoreceptors. Consistent with ONL thinning, quantification of OS length also revealed a significant reduction at 12 months and near-complete loss by 21 months (Fig. 3E, F). We, however, did not detect any alterations neither in thickness of ONL/INL nor OS length in heterozygous *Gm20541$^{SKO}$* (*Gm20541$^{flox/+}$;* Six-Cre) mouse retina, compared to those in control littermates (Figure S4), in line with the unaffected parents in described RP family.

Given that impaired visual function and significant thinning of ONL were detected in *Gm20541$^{SKO}$* mice, we next focused on profiling the pathological details of retinal photoreceptors. Immunostaining using retinal sections from 12-month-old mice was performed against antibodies of Rhodopsin (rod OS marker) and NaK pump (rod IS marker) to analyze the subcellular changes in rods. Although the Rhodopsin labeled OS was well organized, the *Gm20541$^{SKO}$* mice showed significantly decreased OS length in central retina, with a nearly 40% reduction compared to that of controls (10.13±0.32 vs 16.76±0.27 mm, *P*=0.00065 by t-test) (Fig. 4A). To further characterize the ultrastructural features of the rod cells in *Gm20541$^{SKO}$* retinas, transmission electron microscopy (TEM) was conducted on 12-month-old retinas and revealed a compact and well-organized OS discs in *Gm20541$^{SKO}$* retinas (Fig. 4B). Moreover, both overall morphology and relative positioning of connecting ciliary structures appeared normal, and no statistic difference (*P*=0.98 by t-test) was detected in the average length of the connecting cilium (CC) and basal body (BB) between

*Gm20541^{SKO}* rods and *Gm20541^{f/f}* controls (Fig. 4C). Consistent with immunofluorescent results, Western blot analysis further confirmed an overall reduction in protein levels of various key molecules in rod OS, including RHO, cGMP-gated cation channel alpha-1 (CNGA1), GPCR kinase 1 (GRK1), protein peripherin 2 (PRPH2), and phosphodiesterase-6-β (PDE6B), in *Gm20541^{SKO}* retinas compared to that of controls (Fig. 4D, E), indicating severe degeneration of rods.

To further examine the pathological changes of cone cells in *Gm20541^{SKO}* mice, we stained retinal sections with the cone OS marker M-opsin and Alexa Fluor-594-conjugated peanut agglutinin (PNA, which labels the cone matrix sheaths). Despite M-opsin was normal localized in the PNA labeled sheaths, a dramatically decrease (16.12±0.32 vs 6.09±0.27 mm, *P*<0.0001 by t-test) in the length of M-opsin marked cone OS was observed in *Gm20541^{SKO}* mice compared to controls (Fig. 4F, G), indicating the occurrence of cone cell degeneration. To precisely characterize the cone amounts in *Gm20541^{SKO}* mice, retinal flat mounts from 12-month-old animals were prepared and coimmunostained with M-opsin antibody and Alexa Fluor-594-conjugated PNA (Fig. 4H). Considering that the M-opsin-containing cones were mainly distributed in the dorsal retina, with very few M-opsin-positive cones in the ventral retina[28], we thus selected the dorsal area for quantitation. Consistent with the immunolabeling results of retinal cryosections, a shortened and misshapen cone OS was observed, accompanied by a slight decrease in the number of M-cones in different dorsal regions were quantified (Fig. 4I), suggesting mild loss of cones in degenerating *Gm20541^{SKO}* retinas. We further examined the retinal phenotype of 12-month-old heterozygous *Gm20541^{SKO}* mice (*Gm20541^{f/+}; Six3-Cre*) and found no statistically significant differences in retinal layer thickness compared to controls (Fig. S5A, B), with little degenerative features in rod and cone cells (Fig. S5C, D).

Given that degenerative features were also observed in other retinal layers in degenerating *Gm20541*[SKO] retinas, phenotypes of the major cell types in the inner retina were also analyzed here. Specifically, immunostaining using retinal bipolar cell (RBC)-specific marker PKCα revealed loss of RBCs in *Gm20541*[SKO] retina compared to that of controls (Fig. S6A). The mean numbers of PKCα-positive cells in the control and *Gm20541*[SKO] mice were 18.58±0.75 and 15.08±0.67 cells/200 μm of retinal length, respectively (Fig. S6B), suggesting a nearly 19% reduction of PKCα-labeled RBCs. However, immunostaining of retinal sections with anti-Brn3a antibody, an RGC-specific marker, (Fig. S6C), showed that RGC number was not statistically significant (*P*=0.26 by t-test) in *Gm20541*[SKO] retinas (Fig. S6D).

Accompanied by the degenerative process, activation of Müller cells, as an indicator of retinal injury[29,30], was also detected by immunostaining with Glial fibrillary acidic protein (GFAP) antibody, which showed a remarkable increase of GFAP signals across from the ganglion cell layer (GCL) to ONL in the degenerating *Gm20541*[SKO] retinas (Fig. S7A). Western blot analysis further confirmed the increased GFAP level in the *Gm20541*[SKO] retina (Fig. S7B, C). Moreover, TUNEL-positive nuclei were occasionally observed mainly in the ONL of degenerating *Gm20541*[SKO] retina, while this is devoid in their control littermates (Fig. S7D, E), demonstrating slow apoptosis of photoreceptor cells. Together, these data indicated that *ZNF124* homologous gene *Gm20541* plays essential roles in the function and homeostasis of the retina, especially in photoreceptors.

**ZNF124 regulates the transcription of *MSX2* through binding its promotor region**

Next, we set out to investigate the potential mechanisms underlying the retinal degeneration and RP occurrence induced by the ZNF124 deficit. As depicted earlier, ZNF124 is a KRAB-ZNF gene containing an array of 7 zinc fingers motifs that are known to binding to specific DNA sequences. Therefore, we aimed to identify the

genomic targets bound and directly regulated by ZNF124 using the Cleavage Under

Targets and Tagmentation (CUT&Tag) approach. Wildtype ZNF124 proteins bearing

a C-terminal FLAG tag were overexpressed in HEK293T cells, followed by

CUT&Tag assay after harvesting (Fig. 5A). In total, we identified 30,453 peaks of

ZNF124 binding in HEK293T cells (Additional file 3), which showed a clear

tendency for ZNF124 enriched regions within 1 kb of the transcriptional start site

(TSS) and weak enrichments at transcriptional end sites (TES) (Fig. 5B, C).

Consistently, analysis of the genic peaks indicates that ZNF124 binds preferentially to

promoters (Fig. 5D): a total of 49.9% (15190) of the peaks map within 3 kb upstream

of the TSS, and over 86.2% (13095) of these promoter peaks localized within 1 kb

upstream of the TSS. A significant number of peaks, however, map to other genome

regions, including intron and intergenic regions (Fig. 5D). To characterize the DNA

consensus sequence recognized by ZNF124, all identified peaks validated by the

MACS program were subjected to *de novo* and known motif analysis using HOMER,

and the top consensus of ZNF124 binding motif was listed in Fig. 5E. Notably, the

typical "TGASTCA" (S=G/C) binding motif was shared between both groups (Fig.

5E, arrows). We then carried out RNA-seq transcriptomic profiling of retinas from 8-

month-old $Gm20541^{SKO}$ mice, which present no obvious retinal degenerative features

during this time. Comparing to control retinas, a total of 375 significantly (|$\log_2$ fold

change|>0.5; $P$<0.05) differentially expressed genes (DEGs) were identified upon

$Gm20541$ deficiency (Fig. 5F, Additional file 4), consisting of 192 up-regulated and

183 down-regulated genes (Fig. 5F). GO enrichment analysis revealed that the DEGs

were primarily associated with the regulation of eye development, eye

morphogenesis, photoreceptor cell differentiation, and transcription factor activity,

implying the essential roles of $Gm20541$ in retina.

To determine which of these are transcriptionally modulated by ZNF124 in our

experimental conditions, we further correlated the CUT&Tag data with RNA-seq

results, and found that 46 genes simultaneously differentially expressed in

*Gm20541[SKO]* retinas and bound by ZNF124 in the promoter region (Fig. 5G). For

reliability, we further employed a previous published ChIP-exo data of 230 KRAB-

ZNF proteins (GEO database: GSE78099)[31], which identified a total of 115 gene

promoters (<3 kb) bound by ZNF124 (Additional file 5). Overlapping genes through

the CUT &Tag, RNA-seq and ChIP-exo data finally indicated that only three genes

(*MSX2, GJA1, WLS*) that are bound by ZNF124 simultaneously showed significantly

altered expression in *Gm20541[SKO]* retinas (Fig. 5G). Interestingly, all these three

targets were significantly downregulated when *Gm20541* was deleted in our RNA

sequencing experiment (Fig. 5H). CUT&Tag data further showed ZNF124 binding to

the promoter regions of these three candidate genes (Fig. 5I). Among the three

candidate genes, MSX2 drew our attention due to its fundamental role in early eye

development—deficiency of which could lead to arrested eye development and

microphthalmia[14,17,32]. We, therefore, selected the MSX2 gene for the following

investigation. As such, we further carried out chromatin immunoprecipitation (ChIP)-

qPCR to investigate evidence of ZNF124 binding on *MSX2* gene promoters, and data

showed that the predicted *MSX2* promoter fragment (-3317/-2995) is the efficient

region for direct ZNF124 interaction (Fig. 5J), suggesting that ZNF124 could

specifically bind this region for transcriptional regulation. Next, we compared the

identified "TGASTCA" (S=G/C) binding motif with the predicted *MSX2* promoter

region (-3317/-2995). As expected, a typical sequence of "TGAGTCA" (-3069/-3063)

in *MSX2* promoter region was aligned with the binding motif (Fig. 5K). To verify

whether ZNF124 activated the *MSX2* promoter, we then constructed reporter plasmids

which contain the predicted *MSX2* promoter fragment (-3317/-2995) upstream of the

Luciferase gene using the pGL4.23 luciferase system (Fig. 5L). Meanwhile, mutant

plasmids were also generated in which the typical "TGAGTCA" (-3069/-3063)

binding sequence was substituted with "GTCTGAC" (Fig. 5L). Consistent with the

observed downregulation of *Msx2* mRNA in *Gm20541[SKO]* retina, the luciferase

reporter assay demonstrated that ZNF124 activated the MSX2 promoter fragment (-3317/-2995) (Fig. 5M). However, the introduction of the "GTCTGAC" mutation in the mutant MSX2 promoter fragments abolished the activation by ZNF124. Thus, these data demonstrated that the "TGAGTCA" (-3069/-3063) region of the MSX2 promoter is critical for its activation by ZNF124. Thereafter, to validate whether ZNF124 binding could regulate MSX2 expression *in vivo*, we applied RT-qPCR to analyze the expression changes in *Gm20541$^{SKO}$* retinas. In line with omics results, the mRNA expression level of *Msx2* in *Gm20541$^{SKO}$* retinas was reduced by over 50% compared to that in controls (Fig. 5N) and this reduction was further validated in protein levels by Western blot analysis using MSX2 antibody (Fig. 5O, P). Taken together, we proposed that MSX2 is an important downstream target of ZNF124 in the retina, which could be modulated by ZNF124 through binding its promotor region.

**MSX2 is essential for function and survival of rod photoreceptors**

*Msx2* encodes for a transcription factor involved in early tissue patterning and dysregulation of which can induce developmental anomalies of several types of tissues, including optic vessel, anterior segment and lens formation during early eye development[33]. To further address the optic abnormalities upon MSX2 depletion, we first constructed a homozygous *Msx2*-deficient (*Msx2$^{-/-}$*) model (Fig. S8A) and then verified the precise excision using Sanger sequencing (Fig. S8B). The deletion was confirmed by RT-PCR (Fig. S8C). Analysis of *Msx2$^{-/-}$* mice at 2-month postnatal ages revealed that these mice displayed dramatic growth retardation when compared with WT littermates, as reflected by significantly smaller body size (Fig. S8D) and lower body weight (Fig. S8E). Besides, *Msx2$^{-/-}$* mice presented progressive hair loss and developed patches of hairiness and baldness (Fig. S8D). Regarding optic features, consistent with previous studies, homozygous *Msx2$^{-/-}$* mice in present study also showed cornea opacity and edema with microphthalmia compared with that of the WT littermates. Enucleated eyes of *Msx2*-deficient mice at 3 postnatal months were

consistently microphthalmia and 50% smaller in size than eyes of WT littermates. Overall, narrowed palpebral fissures, smaller eyeballs, and cornea edema were detected in the *Msx2*-deficient mice. Such phenotypes became more apparent after the eyelids opened (Fig. S8F). Histologic analysis of the eyes at 3 postnatal weeks disclosed thickened cornea, iridocorneal adhesion, iris hyperplasia, and smaller lens in the anterior segment compared with that of the WT littermates (Fig. S8G). Meanwhile, we also found that the cerebellum morphology of *Msx2*$^{-/-}$ mice was markedly smaller than their age matched littermates, presenting severe atrophy compared to other brain regions (Fig. S8H). This observation was confirmed by histologic study of cerebellar sections (Fig. S8I), suggesting impeditive cerebellar development.

These data highlighted key regulating effect of MSX2 in the development of the vertebrate eye and other tissues. We, subsequently, asked whether the retinal dystrophy observed upon ZNF124 abrogation in human and mice could also be detected in *Msx2* deficiency mice. However, the microphthalmia observed in *Msx2*$^{-/-}$ mice presents a challenge in investigating the role of MSX2 in the neuroretina. We, therefore, further generated *Msx2* rod conditional knockout (*Msx2*$^{RKO}$) mice by mating *Msx2*$^{f/f}$ with Rhodopsin promoter-driven Cre transgenic mice (Fig. 6A), and genotyped them using RT-PCR (Fig. 6B). The excision efficiency of *Msx2* in rods was valeted by Western blot using protein lysis extracted from retinal samples, which revealed that the expression level of MSX2 in *Msx2*$^{RKO}$ mouse retina was reduced to ~43% of that of control (Fig. 6C). Considering that MSX2 may also be expressed in other retinal cell types, the excision efficiency of *Msx2* in rod cells was fairly robust. Thereafter, histologic analysis was performed to examine the retinal morphology in *Msx2*$^{RKO}$ retinas at different ages. At 2 and 4 months of age, *Msx2*$^{RKO}$ retina appeared normal compared to their corresponding *Msx2*$^{f/f}$ littermates (Fig. S9A, B), while a slightly thinning of the ONL began to present in the retina of 5- (Fig. 6D) and 6-

16

month-old (Fig. S9C) $Msx2^{RKO}$ mice. This phenotype became pronounced in $Msx2^{RKO}$ mice at 9 months of age, with an average 43.5% decrease in the thickness of ONL accompanied by shorted OS, while no obvious difference was observed in the inner retinal layers between $Msx2^{RKO}$ and their control $Msx2^{f/f}$ littermates (Fig. 6E). Along with the reduction in ONL thickness, the length of the OS also decreased in 5-month-old $Msx2^{RKO}$ mice, with a more pronounced shortening observed at 9 months compared to controls (Fig. 6D, E). Immunostaining data showed that RHO and PDE6B were correctly localized to the shortened OSs of 9-month-old $Msx2^{RKO}$ mice (Fig. 6F). Moreover, reactive astrogliosis were also detected in degenerating $Msx2^{RKO}$ retinas by immunostaining with GFAP antibody (Fig. 6G), indicating extensive retinal damage. The retinal morphology of heterozygous $Msx2^{RKO}$ mice ($Msx2^{loxP/+}$; $Rho$-$Cre$) was also assessed here. However, unlike significant retinal degeneration in homozygous $Msx2^{RKO}$ mice (Fig. S9D), no visible retinal degenerative feature was observed by 11 months of age (Fig. S10). Together, these data suggest that MSX2 also plays roles in the neuroretina, and the excision of which in rod photoreceptors could lead to retinal degeneration, mimicking the effects of $ZNF124$ ($Gm20541$) deficiency.

**ZNF124 maintains normal photoreceptor function by regulating expressions of**
**$Rs1$, $Pde6g$ and $Pdc$ via MSX2 axis**

To dissect the molecular mechanism underlying MSX2 regulation of photoreceptor survival, we performed bulk RNA-seq analysis on total retinal RNAs extracted from the 4-month-old $Msx2^{RKO}$ and $Msx2^{f/f}$ mice to compare the gene expression profiles. Among the 17838 genes expressed, transcripts of 958 (5.4%) genes were upregulated, whereas transcripts of 496 (2.8%) genes were downregulated in $Msx2^{RKO}$ mice compared to the controls (Fig. 7A, Additional file 6). Gene ontology (GO) enrichment analysis demonstrated the top most significantly affected categories in genes that were downregulated as a result of $Msx2$ depletion. In keeping with the rod dysfunction after

*Msx2* deletion, among the top downregulated gene clusters were associated with photoreceptor inner and outer segments, photoreceptor cell maintenance, phototransduction and visual perception process (Fig. 7B). Strikingly, a subset of retinal dystrophy associated genes was downregulated in *Msx2^{RKO}* cells (Fig. 7B). Among them, several known regulatory genes of visual perception, such as *Prph2, Pde6g, Reep6, Rgs9bp* and *Gnat1*, were identified. In order to elucidate how loss of ZNF124 (Gm20541) could cause retinal degeneration through regulation of MSX2, we compared downregulated transcripts that were enriched in visual perception process upon MSX2 depletion to those simultaneously down-regulated ($|\log_2$ fold change$|<0$; $P<0.05$) in *Gm20541^{SKO}* retinas, and revealed that four genes (*Rs1, Pde6g, Ush2a*, and *Pdc*) were shared (Fig. 7C). Gene-expression heatmaps and statistics of the RNA-seq data from both *Msx2^{RKO}* and *Gm20541^{SKO}* strains revealed that mRNA expressions of these selected genes were significantly downregulated in the *Msx2^{RKO}* retinas, while showing varying degrees of reduction in *Gm20541^{SKO}* retinas (Fig. 7D, E). RT-qPCR further validated these findings, showing a significant decrease ($P<0.001$) in mRNA levels of *Rs1*, *Pde6g*, and *Pdc* in Msx2^{RKO} retinas, while *Ush2a* exhibited no statistically significant change (Fig. 7F). Consistent with the transcriptional results, Western blot analysis confirmed a 45%, 46%, and 47% reduction in RS1, PDE6G, and PDC protein levels, respectively, in *Msx2^{RKO}* retinas compared to those of controls (Fig. 7G, H). These findings suggested that the reduced MSX2 content due to Gm20541 deficiency subsequently downregulated expression levels of murine homologues of retinal dystrophy associated genes *Rs1*, *Pde6g*, and *Pdc* in the retina. This dysregulation ultimately contributes to progressive retinal degeneration and impaired visual function, providing a molecular basis for retinal dystrophy associated with ZNF124 deficiency in both humans and mice.

## Discussion

In the current study, we report a novel homozygous splicing mutation (c.219-1delG) of *ZNF124* gene in a family suffering from RP. Detailed cDNA analysis demonstrated a 9 bp skipping across exon 3 and 4 in the patient's *ZNF124* transcript. To investigate the in vivo roles of ZNF124 in retina, we first confirmed *Gm20541* as the homologous gene of *ZNF124* in mice, and following knockout study of this murine homologous gene manifested an RP-like phenotypes characterized by reduced electroretinogram response and late-onset retinal degeneration in mice, highlighting the essential roles of ZNF124 in both human and mouse retina and RP pathogenesis. As one of the members of this family, ZNF124 contains 7 predicted C2H2-type fingers thought to be implicated in DNA binding, and act as a transcriptional regulator linked to cell survival and tumorigenesis in several cellular contexts. Increased expression of *ZNF124* was detected after vascular endothelial growth factor (VEGF) stimulation in human leukemia cell lines and results in inhibition of apoptotic cell death[10]. In the nervous system, loss of ZNF124 has been linked to defects in cerebellar development[13]. Here, we identified a novel homozygous splicing mutation c.219-1delG in the ZNF124 gene associated with RP pathologies (Fig. 1E, F). This splicing mutation resulted in a frameshift change at the 73rd Serine and a termination codon occurred after twenty amino acid (p.S73fs20*), which finally caused truncation of the ZNF124 protein from its C-terminal (Fig. 1J). Thus, our data implicated, for the first time, the crucial roles of ZNF124 in human RP pathologies. A limitation of the current study is the identification of the novel *ZNF124* variant solely within a single consanguineous family. While the co-segregation, functional studies, and mouse model strongly support the pathogenicity of this gene, further investigation and validation are required to confirm the broader involvement of *ZNF124* in RP pathogenesis, involving screening a larger cohort of independent families or sporadic cases to identify *ZNF124* mutations and more comprehensively establish its association with inherited retinal dystrophies.

After alignment, *Gm20541* was selected as the closest homolog of the human counterpart in murine genome (Fig. S2A). So far, regrettably, no literature report elaborates on the biological function of *Gm20541* as a stand-alone gene, and only few omics datasets point towards the association of *Gm20541* with various biological processes. Interestingly, *Gm20541* is controversially considered as a pseudogene between different databases. Here, we detected distinct transcriptional expression of *Gm20541* in mouse brain, cerebellum, liver, retina, intestine, muscle, heart, kidney and spleen (Fig. S2B, C). Subsequent western blot analysis of tissue lysis from *Gm20541*$^{f/f}$ mouse further confirmed the robust protein expression in the heart, liver and retina (Fig. S2B), demonstrating the *Gm20541* could be translated as a functional protein. We, subsequently, revealed that *Gm20541* paly essential role in retinas, as showed by the progressive degeneration of *Gm20541* deficient retina, especially in the photoreceptor layers (Fig. 4A-C), mimicking the human RP pathologies. Interestingly, compared to the clinical phenotypes of patients carrying mutations in ZNF124, the phenotype of our *Gm20541*$^{SKO}$ mice is rather mild. Actually, it is not uncommon to observe differences in mouse knockout phenotypes and human patient clinical phenotypes. One such example is the phenotypes of *CRB1* patients and *Rd8* mice. Mutations in *CRB1* lead to LCA8, retinitis pigmentosa 12 or childhood- and juvenile-onset rod-cone and cone-rod dystrophy[34-36]. Most patients exhibited early-onset severe vision loss. Interestingly, a new mouse model, retinal degeneration-8 (*rd8*), with a single base deletion in the mouse *Crb1* gene was generated[37]. *rd8* mutation resulted in a frameshift and premature stop codon, and the truncated protein lost the transmembrane and cytoplasmic domains of CRB1. However, *rd8* homozygous mutant mice only exhibited mild retinal degeneration, and photoreceptor degeneration was observed only within spotted regions of the retina, which implies that the severity of retinal pathology is dependent on genetic backgrounds[38,39]. Taking these into consideration, there might be some discrepancy between the phenotypes of *ZNF124* mutation carrying patients and those of *Gm2054* knockout mice.

Indeed, ZNF124 should simultaneously regulates a subset of genes in different retinal cell types, as our observation that varying degrees of loss in other retinal cells in *Gm20541^(SKO)* retinas, such as cones, RBCs, and RGCs (Fig. S6). Although some literature indicated that prolonged degeneration of rod photoreceptors could induce the comprehensive degeneration of other retinal cells[40,41], considering that the phenotype of photoreceptor dystrophy in the 12-month-old *Gm20541^(SKO)* mice is still relatively mild (Fig. 4B), the loss of other retinal cells observed at this stage should be directly attributed to the absence of ZNF124 instead of the secondary effect of rod loss. This notion can be further supported by the evidence from our immunofluorescent data and the single cell database that ZNF124 is broadly expressed in different retinal cells (Fig. S2A, B). In addition, we also observed the defects in limb development in pan-knockout *Gm20541^(KO first)* mice (Fig. S4B), hinting at the possibility of a more general role for ZNF124 in morphogenetic process. However, histological examination of 8-month-old *Gm20541^(KO first)* retinas revealed no detectable retinal developmental abnormalities (Fig. S4C), indicating that ZNF124 deficiency does not affect retinal maturation. Indeed, whether subtle abnormalities exist in other systems remains unknown, thus warranting further investigation.

Another key finding from our study is that ZNF124 could regulate MSX2 expression through a direct binding of its specific promoter region (Fig. 5I-P). MSX2 belongs to the MSX gene family, which acts as both a transcriptional repressor and activator whose normal activity may establish a balance between survival and apoptosis[42]. For instance, previous reports demonstrated that germline knockouts *Msx2^(−/−)* mice exhibited microphthalmia commit with small lens formation or even aphakia, as well as a persistent lens stalk and iris hyperplasia in the anterior segment[20], while overexpression of which in mice could also lead to optic nerve aplasia and

microphthalmia[17], suggesting that the precise regulation of MSX2 expression is critical for ocular development. Consistent with these findings, our homozygous *Msx2*^{-/-} mice also showed narrowed palpebral fissure, cornea opacity and edema with microphthalmia compared with that of the WT littermates (Fig. S8F). By constructing *Msx2* rod-specific knockout mouse, we further revealed an apparent thinning of retinal ONL owing to comprehensive degeneration of rod cells in this mouse line (Fig. 6D, E). Notably, the degenerative phenotype of *Msx2*[RKO] mice manifested much earlier than that of the *Gm20541*[SKO] mice. This discrepancy in the age of onset likely stems from the partial loss (∼60% reduction) of *Msx2* expression in the *Gm20541*[SKO] retina (Fig5. N-P), which is insufficient to trigger early-onset pathogenesis. However, our data further showed that no observable retinal phenotype was detected in heterozygous *Msx2*[RKO] (*Msx2*[loxP/+]; *Rho-Cre*) mice at 6 or 11 months of age (Fig. S10), suggesting a potential dosage-compensation effect of MSX2 as a transcription factor in the retina. Moreover, since *Gm20541*[SKO] mice begin to show mild retinal degeneration at 12 months (Fig. 3), it is plausible that ZNF124 also regulates the expression of other retinal proteins, such as GJA1 and WLS identified through our multi-omics analysis (Fig. 5G, H), which may collectively contribute to the late-onset retinal degeneration phenotype. Mechanistically, combined analysis of bulk RNA-seq data from *Gm20541* and *Msx2* mutant retinas finally unveils that MSX2 act as the transcriptional activator of *Rs1*, *Pde6g* and *Pdc* genes in retina (Fig. 7). Intriguingly, in humans, *RS1*, *PDE6G* and *PDC* are associated with severe retinal dystrophy diseases, with both *PDE6G* and *PDC* are well-known RP-causing genes[4], and mutations in *RS1* cause X-linked retinoschisis (XLRS), an early onset macular degeneration characterized by a splitting of the retina[43]. Specifically, RS1 is expressed and secreted from photoreceptors and bipolar cells as a homo-octameric complex, and its functions are related to cell adhesion and maintenance of retinal structure integrity[44,45]. Currently, seven mouse models have been established and effectively mimicked key features of XLRS patients, including typical retinal abnormalities[46].

*Pde6g* encodes the gamma subunit of Rod-specific phosphodiesterase 6 (PDE6) complex, which is composed of alpha- and beta-catalytic subunits and two inhibitory gamma subunits[47,48], serve as an essential component of the visual transduction cascade. Animal model studies also indicated that *Pde6g* depletion could lead to very early and rapid degeneration of rod photoreceptor cells, with only a single row of cone photoreceptor nuclei remaining by P16[49], highlighting the crucial roles of PDE6G in retinas, especially in rod photoreceptors. The third targeted gene *PDC* is associated with RP and Usher syndrome type II[50], and PDC protein is located in the outer and inner segments of rod cells and participates in the regulation of visual phototransduction and photoreceptor metabolism[51]. In mice, loss of *Pdc* gene causes a reduction in the cellular levels and mislocalization of the Transducin in rod photoreceptors, which finally leads to retina degeneration[52,53]. Our findings, coupled with the above published observations, provide evidence that disruption of MSX2 regulation on *Rs1*, *Pde6g* and *Pdc* could influence the retinal function and stability, demonstrating, for the first time, the pivotal roles of MSX2 in the function and survival of neuroretinas. The elucidation of the ZNF124-MSX2 axis in our study also provides a promising way for the development of targeted therapeutic strategies for ZNF124-associated RP. Restoring the expression of downstream target genes, such as *MSX2* or its regulated retinal dystrophy-associated genes, may mitigate photoreceptor degeneration and preserve retinal function. Gene therapy approaches, including AAV-mediated overexpression of ZNF124 or MSX2 could potentially re-establish protective transcriptional networks disrupted in RP. Additionally, pharmacological interventions aimed at modulating the activity of this axis may offer alternative therapeutic options. Thus, our work provides the theoretical basis for gene therapy and pharmacological intervention for the ZNF124-associated IRDs.

In summary, our study identifies ZNF124 as a novel gene associated with arRP in human patients and demonstrates that its deficiency leads to comprehensive retinal

degeneration and vision loss in knockout mouse models, supporting that ZNF124 plays essential functions in the human retina. Through multi-omics analysis, we further uncovered that MSX2 is a novel downstream player of ZNF124 to mediate normal retinal homeostasis and visual function through modulating the expression of retinal dystrophy genes *RS1*, *PDE6G*, and *PDC*. In summary, our study discovered a novel ZNF124 mutation linked to human RP and demonstrated a novel regulating mechanism for retinal dystrophy pathogenesis.

# Materials and Methods

## Patient recruitment and whole exome sequencing (WES)

This research was carried out in accordance with the tenets of the Declaration of Helsinki, and approved by the Institutional Ethics Review Boards of the Sichuan Provincial People's Hospital and Aravind Eye Hospital (Madurai, Tamil Nadu, India). Written informed consents were obtained from the patients and their family members involved in this study. The probands and the related family members were clinically diagnosed at Sichuan Provincial People's Hospital. Peripheral blood samples were collected from probands and their family members. Ophthalmic examinations were executed, including peripheral vision test, fundus photographic examination, and visual electrophysiological analysis.

For whole-exome sequencing (WES), peripheral blood from the patient and unaffected relatives were collected in EDTA anticoagulant tubes and then genomic DNA was isolated using DNA extraction kits according to the manufacturer's instructions (TianGen, Beijing, China). The subsequent details of library construction, sequencing analysis of DNA samples to identify candidate pathogenic genes for RP patients were carried out as previously described[22,23]. Validation of the mutations in patients and their relatives was performed by Sanger sequencing.

**Sanger sequencing analysis**

Specific PCR primers (Supplementary Table S1) were designed and synthesized by Sangon Biotech (Shanghai, China) to amplify genomic DNA or cDNA fragments. The PCR products were purified by FastAP Thermosensitive Alkaline Phosphatase (Thermo Scientific Fermentas, Waltham, MA, USA), and then were directly sequenced using BigDye version 3.1 and an ABI 3730 automated sequencer (Applied Biosystems, Foster City, CA, USA) according to the manufacturer's instructions. The sequencing results were collated using Chromas software.

**Mouse models**

All animal experiment protocols were approved by the Institutional Animal Care and Use Committee of Sichuan Provincial People's Hospital (Chengdu, Sichuan, China) (Approval number: LS-20180063) and conducted in accordance with the ARVO Statement for the Use of Animals in Ophthalmic and Vision Research. All mice were housed in a controlled environment with a temperature of 24±2℃ and a 12-hour light/dark cycle, with free access to food and water. Mice were maintained on a C57BL/6J background.

The *Gm20541*-knockout first mice were generated by traditional method. Briefly, the *Gm20541*-knockout (KO) first targeting vector, which contains a gene trap (GT) cassette inserted into intron 2 and floxed exons 3 with a Flag tag (See Fig. 2A for diagram) was constructed. The targeting vector was transfected by electroporation of mouse 129S4 embryonic stem cells. Homologously recombined positive clones were selected by neomycin, and screened by PCR. After that, two independent clones of the targeted stem cells were microinjected into C57BL/6J blastocysts. Resulting chimaera male mice were mated to C57BL/6 J female mice to generate F1 heterozygous founders. Heterozygous F1 mice were crossed to generate F2 off-spring. To generate a conditional allele of *Gm20541*, heterozygous F1 mice were crossed to flippase

(FLP) mice (strain name: *B6.129S4-Gt(ROSA)26Sortm1(FLP1)Dym/RainJ*, JAX

stock number: 009086) to remove the FRT-flanked IRES-GFP reporter and neomycin

cassette. The resulting conditional allele of Gm20541 was backcrossed to C57BL/6J

for 5 generations and designated as B6.129S4-*Gm2054$^{em1Zxj}$* (*Gm20541$^{flox/flox}$*,

*Gm20541$^{f/f}$*). Thereafter, *Gm20541$^{f/f}$* mice were mated to Six3-Cre line (Jackson

Laboratory Stock Tg(Six3-cre)69Frty/GcoJ, stock no. 019755) to generate retina-

specific knockout *Gm20541$^{f/f}$; Six-Cre* mice (hereafter referred to as *Gm20541$^{SKO}$*).

*Msx2* KO strain was purchased from Cyagen (Suzhou, China, Strain S-KO-17369).

Homozygous KO mice were generated by intercrossed heterozygous *Msx2* mice.

Mice with *Msx2* deletion specifically in retinal rods were generated using the Cre-

loxP system. Briefly, *Msx2$^{flox/flox}$* mice were purchased from GemPharmatech

(Nanjing, China), which were crossed with *B6.Cg-Pde6b<+> Tg(Rho-icre)1Ck/Boc*

(Jackson Laboratory, stock no. 015850) transgenic mice to yield progeny with the

genotype *Msx2$^{flox/+}$; Rho-Cre*. Then, the *Msx2$^{flox/+}$; Rho-Cre* mice were crossed with

*Msx2$^{flox/flox}$* animals to generate *Msx2$^{flox/flox}$; Rho-Cre* (*Msx2$^{RKO}$*) mice. *Msx2$^{flox/flox}$*

(*Msx2$^{f/f}$*) littermates were used as controls. All the mice were housed in ventilated,

specific pathogen-free, and thermostatic conditions with a 12-h light-dark cycle at

24°C.

**Genotyping**

Mouse genomic DNA samples were extracted from mouse tails and genotyped using

PCR. The knockout alleles of *Gm20541* or *Msx2* were genotyped using the

corresponding primers (Supplementary Table S1). All amplification reactions were

performed using a master mix (Invitrogen, CA, USA) according to the manufacturer's

instructions. The first cycle of PCR consisted of holding at 95°C for 5 minutes,

followed by 32 cycles of 95°C for 15 seconds, 60°C for 30 seconds and 72°C for 30

seconds. The PCR products were separated by DNA electrophoresis on a 3% agarose gel.

**Histological analysis**

For hematoxylin and eosin staining (H&E), enucleated eyes were fixed overnight in 1.22% glutaraldehyde and 0.8% paraformaldehyde in 0.08 M phosphate buffer, embedded in paraffin and then cut into 5 μm sections. To ensure that sections used for quantification came from the same eccentricity, the globe was embedded in the same orientation. Sections that encompassed the optic nerve (ON) were selected for staining with H&E according to a standard protocol. The slices were scanned by Pannoramic DESK (3D HISTECH) and visualized or measured using CaseViewer 2.4 software (3D HISTECH). The thickness of ONL was measured every 250 μm from ON. Measurements were obtained from at least three sections from three mice of each genotype and averaged.

**Electroretinography (ERG)**

For electroretinographic evaluation, following overnight dark adaptation, mice were anesthetized with an intraperitoneal injection of xylazine (80 mg/kg) and ketamine (16 mg/kg) in normal saline. Thereafter, the pupils were dilated using one drop of 0.5% tropicamide phenylephrine, and one drop of 0.5% oxybuprocaine hydrochloride was administered for local anesthesia. The animals were placed on a heating pad during the ERG procedure. All handling, preparation, and electrode placements were performed under dim red light to maintain dark adaptation. ERG was performed by using an instrument set of Roland electroretinogram recorder and Ganzfeld Q450 stimulator (Roland Consult. Heidelberger. Germany). Dark (scotopic) ERG was performed firstly, with a serial of 0.03, 0.3, 3.0, and 20.0 cds/m$^2$ stimulating luminance used in order. After that, a light adaptation period lasting for 10 min was

instituted before the photopic response assessments. Photopic 3.0 ERG, 20.0 ERG, and photopic 20.0 flicker responses were recorded under corresponding stimulations.

**Immunohistochemistry**

For immunohistochemistry, eyes were removed from euthanized mice by intraperitoneal injection of pentobarbital (75 mg/kg) and by cervical dislocation. and fixed in 4% paraformaldehyde in 100 mM phosphate buffer (pH 7.4) for 1 hour at 4°C, followed by cryoprotection in 30% sucrose for 2 hours. The lenses were removed, and the eyes were embedded in optimal cutting temperature (OCT) solution and sectioned at a 10 μm thickness. After blocking and permeabilization with 10% normal donkey serum and 0.2% Triton X-100 in phosphate buffer for 1 hour, the sections were labeled with the primary antibody overnight at 4°C. The primary antibodies used are shown in Supplementary Table S2. The sections were rinsed in PBS three times, Alexa Fluor 594/488-conjugated goat anti-mouse/rabbit secondary antibody (Cat# A11005 and A11008, Invitrogen, Waltham, MA, USA, 1:500 dilution) was applied, and nuclei were counterstained with DAPI (Cat# D8417, Sigma, St Louis, MO, USA) for 1 h at room temperature. Images were captured on a Zeiss LSM 800 confocal scanning microscope. In addition, the fluorescence intensity was quantified using ZEN 2.3 imaging software.

**Retinal flat mounts and Quantification of cone cells**

Retinal whole mounts were prepared as previously described[30,54]. Briefly, retinas were dissected from enucleated eyes and flattened, which were immersed in 4% PFA for 24h at 4 °C, then blocked in PBS containing 1% bovine serum albumin and 0.5 % Triton X-100 and incubated with polyclonal rabbit anti-Brn3a antibody for 12 h at 4 °C. After several washes, the retinas were incubated with the secondary antibody, AlexaFluor 488-conjugated goat anti-rabbit secondary antibody (Cat#A11008, Invitrogen, Waltham, MA, USA, 1:250 dilution) for 4 h at room temperature, and

subsequently washed with PBS. To precisely quantitate the loss of Cone cells, the dorsal-ventral orientation of each retina was determined using previously described instructions[30,54], and the retina was then subdivided into 2 sectors with radii of 1 mm and 2 mm. Cones were counted in the dorsal squares in each sector to determine the average cone density (cones/mm$^2$).

**Transmission electron microscopy (TEM)**

TEM used for detecting rod degenerative characterization was performed as previously described[30]. The sections were imaged under a Philips CM120 scanning transmission electron microscope.

**TUNEL assay**

The terminal deoxynucleotidyl transferase-mediated biotinylated UTP nickend labeling (TUNEL) assay was used to detect the apoptotic cell death according to the manufacturer's instruction (Roche Diagnostics, Indianapolis, IN, USA) on retinal frozen sections. Images were captured by Zeiss LSM 900 confocal scanning microscope.

**Western blot analysis**

Protein samples were prepared and subjected to SDS-PAGE analysis as previously described[30]. The primary antibodies used are shown in Supplementary Table S2. The relative intensity of the immunoreactive bands was quantified using the gel analysis tool provided in ImageJ software. The intensity of the proteins of interest was normalized to that of GAPDH. At least three independent Western blots were conducted, and one typical blot is presented. The uncropped images were shown in Additional file 7.

**RNA extraction and RT-qPCR**

Retinal total RNA was extracted using TRIzol reagent (Cat# T9424, Sigma, Saint Louis, MO, USA) as recommended by the manufacturer. First-strand cDNA was synthesized using an iScript cDNA Synthesis Kit (Cat# 170-8890, Bio-Rad, Hercules, California, USA). Quantitative PCR was carried out using iTaq SYBRMix (Cat# 1725120, Bio-Rad, Hercules, California, USA) and a CFX384 Touch Real-Time PCR Detection System (Cat# BJ005303, Bio-Rad, Hercules, California, USA). Primers were designed using Primer3Plus or obtained from published resources. Supplementary Table S1 shows the specific primer sequences used. All target genes were normalized to actin mRNA levels, and the fold change was calculated by performing delta-delta Ct analysis.

**RNA-sequencing**

RNA sequencing was performed as before[30]. After harvest, two retinas from one mouse were collected as a sample, which was frozen immediately and sent to Seqhealth Corporation Inc. (Wuhan, China) for high-throughput RNA seq on an Illumina HiSeq 2500 platform generating 150 bp paired-end reads. All gene expression values from RNA-seq were converted to related log2 values for further analyzed. A *P*-value no more than 0.05 was considered to be significant.

**CUT&Tag sequencing**

In order to study the targeted genes of ZNF124, we employed CUT&Tag sequencing using ZNF124 overexpressed HEK293T cells. $1 \times 10^5$ HEK293T cells with pcDNA-ZNF124-Flag transfected were prepared and sent to Personalbio Inc. (Shanghai, China) for CUT&Tag assay, which was performed as described previously with modifications[55]. In brief, cells were prepared and immobilized on concanavalin A beads. Beads are incubated with a Flag primary antibody (F1804, Sigma), followed by incubation with a secondary antibody anti-Mouse IgG (Millipore cat.no. 12-371). Beads were washed and incubated with pA-Tn5. Tn5 was activated by addition of

$Mg^{2+}$ and incubated at 37°C for 1 h. Then cells were resuspended in tagmentation buffer (10mM MgCl2 in Dig-med Buffer) and incubated at 37 °C for 1 h. DNA was purified with phenol-chloroform-isoamyl alcohol extraction and constructed CUT&Tag library according to the manufacturer's instructions. Library was quantified by Equalbit dsDNA HS Assay Kit (Vazyme, EQ111-01) using Qubit™ 4 Fluorometer (Invitrogen, Q33226). Libraries were subjected to paired-end 150 bp sequencing in the Illumina Novaseq 6000 platform following the manufacturer's instructions.

**Cell culture and transfection**

HEK293T cells were purchased from National Infrastructure of cell line Resource (Wuhan, China) and were recently authenticated by STR profiling. They were cultured in DMEM with high glucose (Hyclone, South Logan, UT, USA) supplemented with 10% fetal bovine serum (Gibco, Grand Island, NY, USA) and 100 U/ml penicillin/streptomycin (Invitrogen, Waltham, MA, USA) in an incubator set to 37°C with 5% CO2. For transfection, cells were seeded in plates (Corning, NY, USA) and transiently transfected with constructed plasmid using Lipofectamine 3000 (Invitrogen, CA, USA) according to the manufacturer's instructions, and the cell lysis were harvested after 48h.

**Chromatin immunoprecipitation (ChIP) qPCR**

A chromatin immunoprecipitation (ChIP) assay was performed using a Magna ChIP Kit (Millipore, Billerica, MA) under manufacturer's instructions. In brief, the suspension containing DNA fragments was sonicated from the empty vector (used as control) or pcDNA3.1-ZNF124-Flag transfected HEK293T cells and collected by centrifugation. A part of suspension soluble chromatin without immunoprecipitation was saved as input DNA. This suspension containing soluble chromatin was then incubated with anti-Flag or IgG antibodies and protein-G/A magnetic beads at 4 °C

overnight. Subsequently, DNA fragment binding with the above antibodies was purified by DNA-purifying slurry and detected by qPCR using primers targeting the specific promoter regions (primer sequences are presented in the Supplementary Table S1).

**Plasmids and luciferase reporter assays**

A human *MSX2* promoter fragment was amplified and cloned into the pGL4.23 basic vector. Mutations in the MSX2 promoter were generated by site-directed mutagenesis. The pcDNA3.1-ZNF124-Flag, pcDNA3.1-MSX2-Flag, and the empty vector were also constructed. All plasmids used in this study were constructed and purchased from Youbao Biotechnology (Changsha, China). The nucleotide sequences of all promoter fragments and mutants were confirmed by DNA sequencing. A Dual-Luciferase Reporter Assay System (Promega, WI) was used to measure luciferase activity. Briefly, cells were harvested 48 hours post-transfection and lysed using cell lysis buffer, followed by incubation on a shaker at room temperature for 5 minutes. The lysates were then centrifuged at 16,000 g for 10 minutes at 4°C. A 96-well microplate was used for the assay. Subsequently, 20 µL of the supernatant was added to each well, followed by 50 µL of Firefly luciferase substrate for activity measurement. Afterward, 50 µL of Renilla luciferase substrate was added for activity measurement. The luciferase activity of each sample was determined by calculating the ratio of Firefly luciferase to Renilla luciferase activity. All luciferase values are shown as mean ± SEM of three independent experiments.

**Statistical analysis**

Each experimental group was repeated three times, yielding at least three independent data points. Statistical analysis was performed using GraphPad Prism 6 software. The data sets were tested for a normal distribution using the Shapiro-Wilk test. For normally distributed data, statistical significance was determined by Student's t-test or

ANOVA. If the data were not normally distributed, a nonparametric statistic was used. p-values were calculated with Student's t-test, one-way or two-way ANOVA followed by Tukey's, Dunnett's or Sidak's multiple comparisons test as appropriate. $P < 0.05$ was considered to indicate statistical significance.

## Competing interest statement

All authors declare that there are no competing interests.

## Author contributions

XZ, ZY, LZ, LH, and PS conceived the project. XZ and ZY designed experiments. YY, XJ, SL, KS, RZ, CC, YS and WL acquired data. YY, LH and XZ analyzed data. YY, PS and XZ interpreted data and drafted the manuscript. XZ, ZY, LZ and SL revised the manuscript. All authors approved submission for publication.

## Data Availability Statement

The data that support the findings of this study are available from the corresponding author upon reasonable request.

## Acknowledgments

## Reference

1.	Hartong, D.T., Berson, E.L. & Dryja, T.P. Retinitis pigmentosa. *The Lancet* **368**, 1795-1809 (2006).
2.	Chang, S., Vaccarella, L., Olatunji, S., Cebulla, C. & Christoforidis, J. Diagnostic challenges in retinitis pigmentosa: genotypic multiplicity and phenotypic variability. *Current genomics* **12**, 267-275 (2011).
3.	Narayan, D.S., Wood, J.P., Chidlow, G. & Casson, R.J. A review of the mechanisms of cone

degeneration in retinitis pigmentosa. *Acta ophthalmologica* **94**, 748-754 (2016).

4.      Daiger, S., Sullivan, L. & Bowne, S. Genes and mutations causing retinitis pigmentosa. *Clinical genetics* **84**, 132-141 (2013).

5.      Sandberg, M.A., Rosner, B., Weigel-DiFranco, C., Dryja, T.P. & Berson, E.L. Disease course of patients with X-linked retinitis pigmentosa due to RPGR gene mutations. *Investigative ophthalmology & visual science* **48**, 1298-1304 (2007).

6.      Neveling, K. *et al.* Next-generation genetic testing for retinitis pigmentosa. *Human mutation* **33**, 963-972 (2012).

7.      Thomas, J.H. & Emerson, R.O. Evolution of C2H2-zinc finger genes revisited. *BMC evolutionary biology* **9**, 1-8 (2009).

8.      Huntley, S. *et al.* A comprehensive catalog of human KRAB-associated zinc finger genes: insights into the evolutionary history of a large family of transcriptional repressors. *Genome research* **16**, 669-677 (2006).

9.      Yang, P., Wang, Y. & Macfarlan, T.S. The role of KRAB-ZFPs in transposable element repression and mammalian evolution. *Trends in Genetics* **33**, 871-881 (2017).

10.     Kuramoto, K. *et al.* ZK7, a novel zinc finger gene, is induced by vascular endothelial growth factor and inhibits apoptotic death in hematopoietic cells. *Cancer research* **60**, 425-430 (2000).

11.     Miyake, N. *et al.* Expression of the Krüppel-type zinc finger gene, ZK7, in head and neck squamous cell carcinoma and normal mucosa. *Cancer letters* **185**, 111-118 (2002).

12.     Luo, Z. *et al.* Genomic and transcriptomic analyses reveals ZNF124 as a critical regulator in highly aggressive medulloblastomas. *Frontiers in Cell and Developmental Biology* **9**, 634056 (2021).

13.     Poot, M. *et al.* Dandy-Walker complex in a boy with a 5 Mb deletion of region 1q44 due to a paternal t (1; 20)(q44; q13. 33). *American Journal of Medical Genetics Part A* **143**, 1038-1044 (2007).

14.     Han, J. *et al.* Concerted action of Msx1 and Msx2 in regulating cranial neural crest cell differentiation during frontal bone development. *Mechanisms of development* **124**, 729-745 (2007).

15.     Antonopoulou, I., Mavrogiannis, L.A., Wilkie, A.O. & Morriss-Kay, G.M. Alx4 and Msx2 play phenotypically similar and additive roles in skull vault differentiation. *Journal of anatomy* **204**, 487-499 (2004).

16.     Zhang, Q. *et al.* Chromatin accessibility predetermines odontoblast terminal differentiation. *Frontiers in Cell and Developmental Biology* **9**, 769193 (2021).

17.     Wu, L.-Y. *et al.* Microphthalmia resulting from MSX2-induced apoptosis in the optic vesicle. *Investigative ophthalmology & visual science* **44**, 2404-2412 (2003).

18.     Foerst-Potts, L. & Sadler, T. Disruption of Msx-1 and Msx-2 reveals roles for these genes in craniofacial, eye, and axial development. *Developmental dynamics: an official publication of the American Association of Anatomists* **209**, 70-84 (1997).

19.     Jiang, S.-Y. & Wang, J.-T. Msx2 alters the timing of retinal ganglion cells fate commitment and differentiation. *Biochemical and biophysical research communications* **395**, 524-529 (2010).

20.     Zhao, J. *et al.* Loss of Msx2 function down-regulates the FoxE3 expression and results in anterior segment dysgenesis resembling Peters anomaly. *The American journal of pathology*

**180**, 2230-2239 (2012).

21. Yu, Z. *et al.* Lens-specific deletion of the Msx2 gene increased apoptosis by enhancing the caspase-3/caspase-8 signaling pathway. *Journal of International Medical Research* **46**, 2843-2855 (2018).

22. Zhou, Y. *et al.* A splicing mutation in aryl hydrocarbon receptor associated with retinitis pigmentosa. *Human molecular genetics* **27**, 2563-2572 (2018).

23. Zhang, L. *et al.* Whole-exome sequencing revealed HKDC1 as a candidate gene associated with autosomal-recessive retinitis pigmentosa. *Human molecular genetics* **27**, 4157-4168 (2018).

24. Corrionero, A., Raker, V.A., Izquierdo, J.M. & Valcárcel, J. Strict 3' splice site sequence requirements for U2 snRNP recruitment after U2AF binding underlie a genetic defect leading to autoimmune disease. *Rna* **17**, 401-411 (2011).

25. Clancy, S. RNA splicing: introns, exons and spliceosome. *Nature Education* **1**, 31 (2008).

26. Uhlén, M. *et al.* Tissue-based map of the human proteome. *Science* **347**, 1260419 (2015).

27. Furuta, Y., Lagutin, O., Hogan, B.L. & Oliver, G.C. Retina- and ventral forebrain-specific Cre recombinase activity in transgenic mice. *genesis* **26**, 130-132 (2000).

28. Eldred, K.C., Avelis, C., Johnston Jr, R.J. & Roberts, E. Modeling binary and graded cone cell fate patterning in the mouse retina. *PLoS computational biology* **16**, e1007691 (2020).

29. Vidal, L. *et al.* Reaction of Müller cells in an experimental rat model of increased intraocular pressure following timolol, latanoprost and brimonidine. *Brain research bulletin* **82**, 18-24 (2010).

30. Yang, Y. *et al.* Mettl14-mediated m6A modification is essential for visual function and retinal photoreceptor survival. *BMC biology* **20**, 140 (2022).

31. Imbeault, M., Helleboid, P.-Y. & Trono, D. KRAB zinc-finger proteins contribute to the evolution of gene regulatory networks. *Nature* **543**, 550-554 (2017).

32. Plaisancié, J. *et al.* MSX2 gene duplication in a patient with eye development defects. *Ophthalmic genetics* **36**, 353-358 (2015).

33. Markitantova, Y. & Simirskii, V. Inherited eye diseases with retinal manifestations through the eyes of homeobox genes. *International journal of molecular sciences* **21**, 1602 (2020).

34. Bujakowska, K. *et al.* CRB1 mutations in inherited retinal dystrophies. *Hum Mutat* **33**, 306-15 (2012).

35. den Hollander, A.I. *et al.* CRB1 mutation spectrum in inherited retinal dystrophies. *Hum Mutat* **24**, 355-69 (2004).

36. den Hollander, A.I. *et al.* Leber congenital amaurosis and retinitis pigmentosa with Coats-like exudative vasculopathy are associated with mutations in the crumbs homologue 1 (CRB1) gene. *Am J Hum Genet* **69**, 198-203 (2001).

37. Mehalow, A.K. *et al.* CRB1 is essential for external limiting membrane integrity and photoreceptor morphogenesis in the mammalian retina. *Hum Mol Genet* **12**, 2179-89 (2003).

38. Aleman, T.S. *et al.* Human CRB1-associated retinal degeneration: comparison with the rd8 Crb1-mutant mouse model. *Invest Ophthalmol Vis Sci* **52**, 6898-910 (2011).

39. Luhmann, U.F. *et al.* The severity of retinal pathology in homozygous Crb1rd8/rd8 mice is dependent on additional genetic factors. *Hum Mol Genet* **24**, 128-41 (2015).

40. Jones, B.W. & Marc, R.E. Retinal remodeling during retinal degeneration. *Experimental eye*

*research* **81**, 123-137 (2005).

41. Strettoi, E., Pignatelli, V., Rossi, C., Porciatti, V. & Falsini, B. Remodeling of second-order neurons in the retina of rd/rd mutant mice. *Vision research* **43**, 867-877 (2003).

42. Ekker, M. *et al.* Relationships among msx gene structure and function in zebrafish and other vertebrates. *Molecular biology and evolution* **14**, 1008-1022 (1997).

43. Tolun, G. *et al.* Paired octamer rings of retinoschisin suggest a junctional model for cell–cell adhesion in the retina. *Proceedings of the National Academy of Sciences* **113**, 5287-5292 (2016).

44. Heymann, J.B. *et al.* Cryo-EM of retinoschisin branched networks suggests an intercellular adhesive scaffold in the retina. *Journal of Cell Biology* **218**, 1027-1038 (2019).

45. Molday, R.S., Kellner, U. & Weber, B.H. X-linked juvenile retinoschisis: clinical diagnosis, genetic analysis, and molecular mechanisms. *Progress in retinal and eye research* **31**, 195-212 (2012).

46. Vijayasarathy, C., Pasha, S.P.B.S. & Sieving, P.A. Of men and mice: Human X-linked retinoschisis and fidelity in mouse modeling. *Progress in Retinal and Eye Research* **87**, 100999 (2022).

47. Baehr, W., Devlin, M.J. & Applebury, M.L. Isolation and characterization of cGMP phosphodiesterase from bovine rod outer segments. *J Biol Chem* **254**, 11669-11677 (1979).

48. Hurley, J. & Stryer, L. Purification and characterization of the gamma regulatory subunit of the cyclic GMP phosphodiesterase from retinal rod outer segments. *Journal of Biological Chemistry* **257**, 11094-11099 (1982).

49. Farber, D.B. & Tsang, S.H. Stationary night blindness or progressive retinal degeneration in mice carrying different alleles of PDE gamma. *Front Biosci* **8**, s666-s675 (2003).

50. Nishiguchi, K.M., Berson, E.L. & Dryja, T.P. Mutation screening of the phosducin gene PDC in patients with retinitis pigmentosa and allied diseases. *Mol Vis* **10**, 62-4 (2004).

51. Lee, R.H., Whelan, J.P., Lolley, R.N. & McGinnis, J.F. The photoreceptor-specific 33 kDa phosphoprotein of mammalian retina: generation of monospecific antibodies and localization by immunocytochemistry. *Experimental eye research* **46**, 829-840 (1988).

52. Sokolov, M. *et al.* Phosducin facilitates light-driven transducin translocation in rod photoreceptors: evidence from the phosducin knockout mouse. *Journal of Biological Chemistry* **279**, 19149-19156 (2004).

53. Krispel, C.M. *et al.* Phosducin regulates the expression of transducin βγ subunits in rod photoreceptors and does not contribute to phototransduction adaptation. *The Journal of general physiology* **130**, 303-312 (2007).

54. Yang, Y. *et al.* A missense mutation in Pitx2 leads to early-onset glaucoma via NRF2-YAP1 axis. *Cell Death & Disease* **12**, 1017 (2021).

55. Kaya-Okur, H.S. *et al.* CUT&Tag for efficient epigenomic profiling of small samples and single cells. *Nature communications* **10**, 1930 (2019).

## Figures legends

**Figure 1. Identification of a *ZNF124* splicing mutation in family with arRP.**

(A) Pedigrees of the family with arRP. Arrows indicated the proband patient, and they were denoted with black symbols. (B) Left panel shows fundus photographs of unaffected controls III:3 and III:4 and patients IV:4 and IV:5. pigmentary deposits were presented in retinas of two patients. The right panel shows representative images of OCT examination. Both probands presented disorganized and thinner retinal layers due to atrophy. (C, D) Visual field test (C) and ERG examination (D) of the proband IV:4, which revealed loss of peripheral vision and weak response to light stimulus in both eyes. (E) Sanger sequencing of the splicing mutation c.219-1G>- in *ZNF124* gene identified in this family, which was co-segregated with the phenotype. Arrows indicate the position of altered nucleotide. Both patients IV:4 and IV:5 harboured the homozygous splicing mutation, and their parents III: 3 and III:4 were heterozygous carriers. (F) Diagram showing the location of the identified ZNF124 splicing mutation in current study. The mutant nucleotide locates at the 3' splice site before exon 4 of *ZNF124* gene. (G) Nucleotide sequence alignment of human ZNF124 and orthologues from other species, depicting a high conservation of c.219-1G>- (encircled in red). (H) Sequence chromatogram of the cDNA samples from probands (IV:4 and IV:5) and control subject, depicting a 10 bp deletion across exon 3-4 of *ZNF124* transcript in probands (IV:4 and IV:5). The deleted bases are marked by red. (I) Diagram showing the location of the deleted base in *ZNF124* transcript, which causes a frameshift variation. (J) Predicted structure of ZNF124. Mutation lies between the KRAB and the first zinc finger motif. The red sequence represents the mis-translated amino acid residues affected by the missense mutation. OS, *oculus sinister*/left eye; OD, *oculus dexter*/right eye.

**Figure 2. Disruption of *ZNF124* homologous gene *Gm20541* in mice led to impaired visual function.**

(A) Schematic showing the targeting strategy for the disruption of the *Gm20541* gene. The knockout (KO)-first allele design is shown a nd a Flag tag was added to the end of exon 3. After recombination by flippase enzyme, the exon 3 is flanked by two loxP sites and finally excised by the Six3-Cre. (B-D) Representative ERG traces corresponding to responses elicited by scotopic (D) and photopic (E, F) conditions at different flash intensity (FI) in mice at 12 months of age. (E, F) Statistical analysis was performed for the amplitudes of a-wave (E), b-wave (F) in scotopic conditions (*n*=4 from 4 mice, two-way ANOVA followed by Tukey's post hoc test). (G) Statistical analysis was performed for the photopic ERG amplitudes and flicker amplitudes in photopic conditions (n=4 from 4 mice, two-way ANOVA followed by Tukey's post hoc test). *$P<0.05$; **$P<0.01$; ***$P<0.001$. ns, no significance. The data are represented as means±SEM.

**Figure 3. Progressive retinal dystrophy in *Gm20541^SKO* mice.**

(A-C) H&E staining of paraffin sections of the *Gm20541^SKO* and corresponding *Gm20541^{f/f}* control retinas at the ages of 8 (A), 12 (B), and 21 months (C). Scar bar: 100 μm. The lower panels show high-magnification images of the boxed areas. Scale bars: 25 μm. (D-F) Quantification analysis of the ONL, INL and OS thickness of the *Gm20541^{f/f}* (*n*=7 from 3 mice) and *Gm20541^SKO* (*n*=6 from 3 mice) retinas from mice at the ages of 8 (D), 12 (E), and 21 months (F). OS, outer segment; IS, inner segment; ONL, outer nuclear layer; INL, inner nuclear layer; GCL, ganglion cell layer. *$P<0.05$; **$P<0.01$; ***$P<0.001$. ns, no significance. The data are represented as means±SEM.

**Figure 4. Degenerative features of rod and cone photoreceptors in *Gm20541^SKO* retina.**

(A) Retinal cryosections from 12-month-old mice were labeled with rod-specific markers rhodopsin (outer segment) and Na-K ATPase (inner segment). DAPI was used to counterstain the nuclei. Scale bars, 25 μm. The panels on the right show high-magnification images of the boxed areas. Scale bars: 10 μm. (B) Representative

transmission electron microscope (TEM) images of photoreceptor outer segments in 12-month-old *Gm20541^{f/f}* and *Gm20541^{SKO}* mice. Scale bar: 1 µm. Higher-magnification images of representative ciliary region are shown in the lower of each genotype. Scale bars: 500 nm. (C) Quantitative analyses of the length of BB and CC between *Gm20541^{f/f}* and *Gm20541^{SKO}* photoreceptors (*n*=10 from 3 mice). (D) Western blot analysis of typical OS proteins in 12-month-old *Gm20541^{f/f}* and *Gm20541^{SKO}* mouse retinas. GAPDH was used as a loading control. (E) Quantification analysis of the protein expression levels (*n*=4 for each genotype). The expression of each protein was normalized to that of GAPDH. (F) Retinal cryosections from 12-month-old mice were labeled with cone markers PNA and M-opsin. DAPI was used to counterstain the nuclei; scale bars, 25 µm. (G) Quantification analysis of the M-opsin marked cone OS length (*n*=12 from 3 mice). (H) Immunostaining of flatmount retinas from 12-month-old mice for M-opsin and PNA markers. Scale bars, 50 µm. Representitive image from dorsal retinal quadrant were shown in the lower panel. Scale bars, 25 µm. (I) Quantification of M-opsin positive cone number per 1mm$^2$ field in *Gm20541^{f/f}* and *Gm20541^{SKO}* retinas (*n*=8 from 3 mice). schematic of retinal flat mount indicating the two sectors (radii: 1 and 2mm) that were used to count cones. OS, outer segment; IS, inner segment; ONL, outer nuclear layer; INL, inner nuclear layer; GCL, ganglion cell layer. *$P$<0.05; **$P$<0.01; ***$P$<0.001. ns, no significance. The data are represented as means±SEM.

**Figure 5. Multi-omics analysis reveals *MSX2* as the downstream target of ZNF124.**

(A) Schematic summary for analysis of ZNF124 target genes. (B, C) Distribution of ZNF124-binding peaks showed strong enrichment within 1 kb upstream of the transcription start sites (TSS). (D) The distribution of ZNF124-binding sites within different gene regions. (E) The consensus sequences of ZNF124-binding sites detected by HOMER motif analysis with CUT&Tag data. The triangle arrows indicate the shared motif between *de novo* and known groups. (F) Volcano plots displaying the differentially expressed genes (DEGs) between *Gm20541^{f/f}* and *Gm20541^{SKO}* retinas

and their statistical significance. Red represents up-regulated genes, blue represents down-regulated genes. (G) Venn diagram of DEGs identified by RNA-seq analysis along with ZNF124 binding genes by CUT&Tag and CHIP-exo data. Three genes were selected according to the overlaps. The RNA-seq and CUT&Tag data was acquired from present study, while the CHIP-exo data were obtained from GEO datasets (GSE78099), which was conducted in published paper.
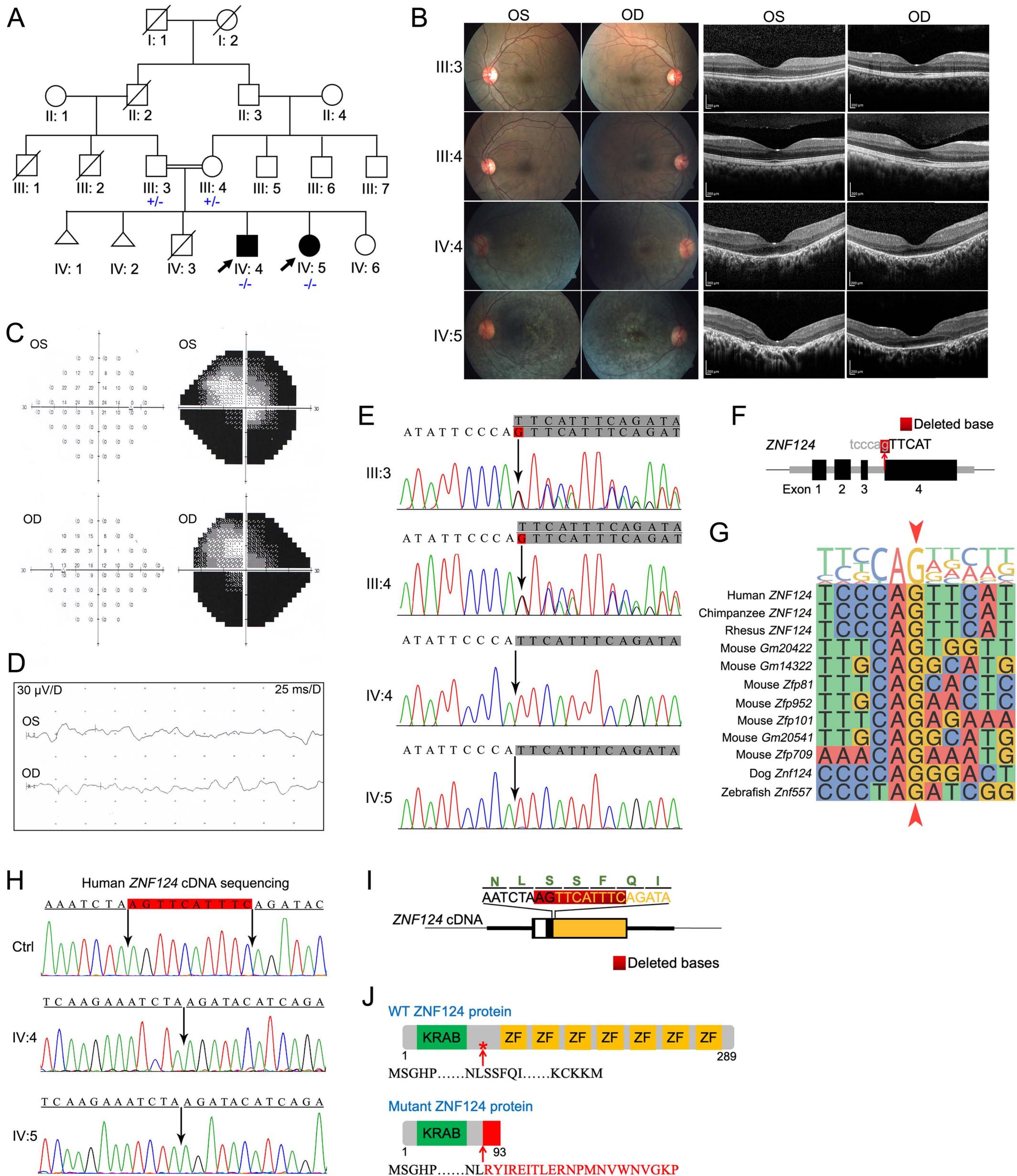
(H) RNA-seq results show that the filtered 3 genes are downregulated in $Gm20541^{SKO}$ retinas. (I) Integrative Genomics Viewer (IGV) tracks displaying the distribution of ZNF124-binding peaks among the filtered genes according to CUT&Tag data. (J) The lower diagram indicates the location of the binding site of ZNF124 in the $MSX2$ gene. The upper panel shows the ChIP-qPCR data of ZNF124 binding to the $MSX2$ promoter using primers as indicated. The HEK293T cells were transfected with the empty vector (used as negative control) or pcDNA3.1-ZNF124-Flag plasmid. Results are presented as the percentage of ChIP/Input ($n$=4 technical replicates). (K) The upper panel shows the typical consensus sequences of ZNF124-binding sites. The lower panel illustrates the sequences of ZNF124-binding sites aligned to the promoter region of the MSX2 gene. The ZNF124-binding sites for ZNF124 are indicated in red letters. The green line refers to the promoter region of MSX2 gene. (L) Schematic diagram of the construction of the pGL luciferase reporter plasmid. The $pRL-TK-hRluc$ plasmid was used as the baseline control. "WT" indicates the aligned ZNF124-binding sites in the MSX2 promoter region, and "Mut" refers to the mutant version of the sequences. (M) The luciferase assay shows that ZNF124 overexpression causes an increase in fluorescence in the wild-type MSX2 promoter group but not in the mutant group. Data were normalized with Renilla luciferase values used as an internal control. (N) RT-qPCR verified the RNA-seq results for the indicated genes ($n$=5 technical replicates). (O) Western blot analysis of the expression of MSX2 in $Gm20541^{f/f}$ and $Gm20541^{SKO}$ retinas. GAPDH was used as a loading control. (O) Quantitative analysis of the expression levels of each subunit, with the statistical comparison between groups ($n$=4 technical replicates). ***$P$<0.001. The data are represented as means±SEM.

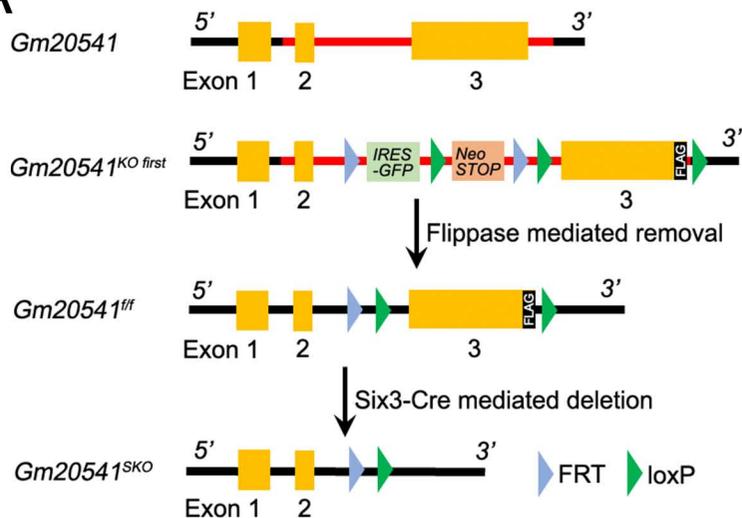**Figure 6. MSX2 is essential for the homeostasis of rod photoreceptors.**

(A) Schematic showing the strategy for generation of *Msx2* rod conditional knockout mice. In the *Msx2* conditional knockout allele, Exon 3 is flanked by two *loxP* sites. When the floxed allele is crossed with the Rho-Cre expressing line, exon3 is deleted, resulting in specific disruption of *Msx2* gene expression in rod cells. (B) Genotyping of $Msx2^{RKO}$ mice. Genomic DNA from mouse-tail lysate of wildtype ($Msx2^{+/+}$), $Msx2^{flox/flox}$ ($Msx2^{f/f}$) and $Msx2^{flox/flox}$; *Rho-Cre* ($Msx2^{RKO}$) mice were amplified using specific primers. (C) Immunoblotting and quantitative comparison of MSX2 protein expression in retinas from $Msx2^{f/f}$ (used as control) and $Msx2^{RKO}$ mice ($n=3$ technical replicates). GAPDH was used as a loading control. (D, E) H&E staining of paraffin sections of $Msx2^{RKO}$ and corresponding controls at the ages of 5 (D) and 9 (E) months. Scale bar: 25 μm. The lower panel shows the quantitative analysis of the ONL and OS thickness of retinas from mice at different ages ($n=8$ from 4 mice). Two-way ANOVA was used for statistical analysis, followed by Tukey's post hoc test. (F) Retinal cryosections from 5-month-old $Msx2^{f/f}$ and $Msx2^{RKO}$ mice were labeled with the OS marker Rhodopsin or PDE6B (green) and IS marker Na-K ATPase (red), respectively. DAPI was used to counterstain the nuclei. Scale bars, 25 μm. (G) Cryosections from the retinas of 5-month-old $Msx2^{f/f}$ and $Msx2^{RKO}$ mice were immunostained for the activated astrocyte marker GFAP (green). Nuclei were counter-stained with DAPI (blue). Scale bars: 250 μm. Higher magnification images of boxed areas were shown in the right panel of each image. Scale bars: 25 μm. OS, outer segment; IS, inner segment; ONL, outer nuclear layer; INL, inner nuclear layer; GCL, ganglion cell layer. *$P$<0.05; **$P$<0.01; ***$P$<0.001. ns, no significance. The data are represented as means±SEM.

**Figure 7. MSX2 maintains photoreceptor function by modulating expressions of *Rs1*, *Pde6g*, and *Pdc*.**

(A) Volcano plots displaying the differentially expressed genes (DEGs) between 4-month-old $Msx2^{f/f}$ and $Msx2^{RKO}$ retinas and their statistical significance. Red represents up-regulated genes, blue represents down-regulated genes. (B) Pathway analysis and significantly enriched GO terms in Biological process (BP), Cellular component (CC) and Molecular function (MF) categories for down-regulated genes in $Msx2^{RKO}$ retinas. (C) Venn diagram of enriched down-regulated genes in visual perception pathway of $Msx2^{RKO}$ retinas and total down-regulated genes in $Gm20541^{SKO}$ retinas. Four genes were overlapped. (D) The heatmap of the expression changes of the filtered four genes in $Msx2^{f/f}$ and $Msx2^{RKO}$ retinas, as well as in $Gm20541^{f/f}$ and $Gm20541^{SKO}$ retinas, as determined by RNA-seq analysis. (E) RNA-seq results showing that the filtered 4 genes were down-regulated in $Msx2^{RKO}$ and $Gm20541^{SKO}$ retinas to varying degrees, compared to corresponding controls. (F) RT-qPCR validated the RNA-seq results for the indicated genes ($n$=4 technical replicates). (G, H) Representative immunoblots (G) and quantification (H) of protein levels in retinas from 4-month-old $Msx2^{f/f}$ and $Msx2^{RKO}$ mice. Protein expression data were normalized according to GAPDH ($n$=3 technical replicates). \*\*\*$P$<0.001. ns, no significance. The data are represented as means±SEM.

A — Gm20541 gene structure with Exon 1, 2, 3; Gm20541 KO first with IRES-GFP, Neo STOP, FLAG; Flippase mediated removal to Gm20541 f/f; Six3-Cre mediated deletion to Gm20541 SKO; FRT and loxP markers.

B — Scotopic ERG; flash intensity (cd·s/m²) 20, 3, 0.3, 0.03; Gm20541 f/f and Gm20541 SKO; 200 µV, 25 ms.

C — Photopic ERG; flash intensity (cd·s/m²) 20, 3; Gm20541 f/f and Gm20541 SKO; 100 µV, 25 ms.

D — Photopic Flicker; Gm20541 f/f, Gm20541 SKO; flash intensity (20 cd·s/m²); 50 µV, 25 ms.

E — a-wave; Scotopic Amplitude (µV); Flash intensity (cd.s/m²) 0.03, 0.3, 3, 20; Gm20541 f/f, Gm20541 SKO; ns, *, **, **.

F — b-wave; Scotopic Amplitude (µV); Flash intensity (cd.s/m²); Gm20541 f/f, Gm20541 SKO; ns, ***, ***, **.

G — Photopic ERG; Amplitude (µV); Gm20541 f/f, Gm20541 SKO; a-wave 3, 20 (ns, ns); b-wave 3, 20 (***, ***); Flicker (***).

A  *Gm20541^{f/f}*  *Gm20541^{SKO}*

OS
IS
ONL
INL
GCL

OS
IS
ONL
INL
GCL

B  *Gm20541^{f/f}*  *Gm20541^{SKO}*

OS
IS
ONL
INL
GCL

OS
IS
ONL
INL
GCL

C  *Gm20541^{f/f}*  *Gm20541^{SKO}*

OS
IS
ONL
INL
GCL

OS
IS
ONL
INL
GCL

D **8 month**

Legend:
- *Gm20541^{f/f}*-ONL    *Gm20541^{SKO}*-ONL
- *Gm20541^{f/f}*-INL    *Gm20541^{SKO}*-INL
- *Gm20541^{f/f}*-OS     *Gm20541^{SKO}*-OS

Thickness (μm)
Distance ON (μm)
Dorsal    Ventral

E **12 month**

Legend:
- *Gm20541^{f/f}*-ONL    *Gm20541^{SKO}*-ONL
- *Gm20541^{f/f}*-INL    *Gm20541^{SKO}*-INL
- *Gm20541^{f/f}*-OS     *Gm20541^{SKO}*-OS

Thickness (μm)
Dorsal    Distance ON (μm)    Ventral

F **21 month**

Legend:
- *Gm20541^{f/f}*-ONL    *Gm20541^{SKO}*-ONL
- *Gm20541^{f/f}*-INL    *Gm20541^{SKO}*-INL
- *Gm20541^{f/f}*-OS     *Gm20541^{SKO}*-OS

Thickness (μm)
Dorsal    Distance ON (μm)    Ventral

A. Volcano plot of Msx2^{RKO} vs Msx2^{f/f}; P-value < 0.05, |log2 (FC)| > 0.5; Up 958, Down 496, No difference 16384.

B. GO enrichment bar chart (GOMF, GOCC, GOBP).

C. Venn diagram of Msx2^{RKO} Enriched genes in visual perception (21) and Down regulated genes in Gm20541^{SKO} retinas (695), overlap 4: Rs1 Pde6g Ush2a Pdc.

D. Heatmap of Rs1, Pde6g, Ush2a, Pdc across Msx2^{f/f}, Msx2^{RKO}, Gm20541^{f/f}, Gm20541^{RKO}.

E. log2 (fold change) bar chart for Rs1, Pde6g, Ush2a, Pdc; Msx2^{RKO} vs Msx2^{f/f} and Gm20541^{SKO} vs Gm20541^{f/f}.

F. Relative mRNA levels (flod change) for Rs1, Pde6g, Ush2a, Pdc; Msx2^{f/f} vs Msx2^{RKO}; ***, ***, ns, ***.

G. Western blot of RS1, PDE6G, PDC, GAPDH; Msx2^{f/f} vs Msx2^{RKO}.

H. Relative protein levels (flod change) for RS1, PDE6G, PDC; Msx2^{f/f} vs Msx2^{RKO}; ***, ***, ***.